



HAL
open science

Contact heating of bi-dispersed milli-beads in a rotary drum. Mechanical segregation impact on temperature distribution and on heating kinetic analyzed by DEM simulation

A. Mesnier, M. Rouabah, C. Cogne, R. Peczalski, S. Vessot-Crastes, P. Vacus,
J. Andrieu

► To cite this version:

A. Mesnier, M. Rouabah, C. Cogne, R. Peczalski, S. Vessot-Crastes, et al.. Contact heating of bi-dispersed milli-beads in a rotary drum. Mechanical segregation impact on temperature distribution and on heating kinetic analyzed by DEM simulation. Powder Technology, 2019, 10.1016/j.powtec.2019.05.059 . hal-02150136

HAL Id: hal-02150136

<https://hal.science/hal-02150136>

Submitted on 25 Oct 2021

HAL is a multi-disciplinary open access archive for the deposit and dissemination of scientific research documents, whether they are published or not. The documents may come from teaching and research institutions in France or abroad, or from public or private research centers.

L'archive ouverte pluridisciplinaire **HAL**, est destinée au dépôt et à la diffusion de documents scientifiques de niveau recherche, publiés ou non, émanant des établissements d'enseignement et de recherche français ou étrangers, des laboratoires publics ou privés.



Distributed under a Creative Commons Attribution - NonCommercial 4.0 International License

Contact heating of bi-dispersed milli-beads in a rotary drum. Mechanical segregation impact on temperature distribution and on heating kinetic analyzed by DEM simulation.

Mesnier, A.^a; Rouabah, M.^a; Cogné, C.^a; Peczalski, R.^{a*}; Vessot-Crastes, S.^a;

Vacus, P.^b; Andrieu, J.^a

^a Univ Lyon, Université Claude Bernard Lyon 1, CNRS, Laboratoire d'Automatique, de Génie des Procédés et de génie Pharmaceutique (LAGEPP), F-69616, Villeurbanne, France.

^b Sanofi Pasteur, 1541 avenue Marcel Mérieux, Marcy l'Etoile, 69280, France.

*E-mail of the corresponding author: roman.peczalski@univ-lyon1.fr

1. Introduction

Modeling and simulation of processes involving stirred beds of particulate solids is a difficult task. The classical macroscopic and continuous medium approach gives a global scope of average trends but does not provide local information which may be critical for some high added-value processes of pharmaceutical bulk products. In most cases, even slight processing discrepancies between individual particles must be avoided. During drying of granular beds, stirring is very often combined with contact heating and the particulate flow mechanics is then coupled with heat transfer. For instance, vacuum contact heating is widely used in the pharmaceutical industry to dry granular products which are sensitive to oxygen and temperature. The vacuum contact drying of stirred powder bed has been firstly

investigated in a macroscopic way (“penetration” model) by Schlünder and Mollekopf [1] for a mono-dispersed and not adhesive granular material. Later, Kwapinska et al. [2] compared the results obtained by the “penetration” analytical method with those obtained by the numerical DEM.

More recently, several authors have independently investigated the effect of operating conditions on mixing and heating rates of rotated beds of monodispersed granular materials. Figueroa et al. [3] have studied various tumbler filling ratios and cross-sectional shapes; Chaudhuri et al. [4] considered various revolution speeds, material types and baffles number and shapes; Gui et al. [5] and Komossa et al. [6] investigated the effect of different revolution speeds; Emady et al. [7] the effect of different revolution speeds and material thermal conductivities; Nafsun et al. [8] considered different revolution speeds and filling ratios. According to this last experimental study, the thermal mixing time, i.e. the time needed for the entire bed composed initially of hot and cold particles to reach a nearly uniform temperature, was decreasing with increasing the rotational speed, or by increasing the number of baffles or by decreasing the filling ratio.

However, industrial materials, even if carefully controlled before processing, are always slightly dispersed in size, or form or composition. Monodispersed beds are textbook reference cases. The major issue industrial R&D engineers are faced with is the transient temperature distribution within dispersed beds composed of particles of different sizes and materials. To our best knowledge, the only publication which dealt directly with thermal dispersion in rotating heterogeneous particulate beds is the second paper of Nafsun et al. [9]. Like in their first paper, the mixing of cold and hot particles was considered, but additionally the influence of different particle size ratio and volume ratio of cold and

hot particles was studied. The thermal mixing time was observed to decrease with increasing the particle size for monodispersed beds. Furthermore, in most of the studied bed compositions the thermal mixing times were found to be higher for bi-dispersed beds than for monodispersed ones.

Rotary mixing of imperfectly monodispersed solid particulate beds unavoidably leads to mechanical segregation, i.e. to accumulation of smaller or/and denser particles in the core of the bed [10]. In our parallel study (results not yet published), radial and axial segregations were experimentally observed for a bi-dispersed bed with two particle sizes or with two particle densities. The radial segregation indexes were measured for different drum filling ratios and for different baffles numbers and heights. The axial segregation index was found to be influenced by the friction coefficient on both drum front and rear walls.

In the case of a bed heated by the lateral cylindrical wall of the rotary drum, which was the situation considered in this work, there exist unavoidably a thermal heterogeneity due to the superficial heat supply. Temperature gradients between the bed core and bed periphery will quickly rise up and then slowly fall down. The evolutions of beads temperature depend on their trajectories and especially on the number of contacts with neighboring particles and with the heating wall. If there is spatial material heterogeneity due to mechanical segregation, it may be expected that the thermal heterogeneity will be enhanced or/and extended in time. This is why mechanical segregation may be suspected to induce additional thermal dispersion called in this paper thermal segregation. In order to quantify separately the effect of mechanical segregation from that of the surface heat source on global thermal dispersion within the bed, a specific thermal segregation index was introduced (see section 2.3) and was used for comparing different morphologies of the bed.

The aim of this paper was first to show the influence of the beds morphologies (mono-dispersed, gaussian-dispersed and bi-dispersed) and baffles configuration (no baffles, short baffles and long baffles) on the thermal homogeneity and global heating kinetic of the bed during mixing and heating inside a rotary drum. Second, the goal was to investigate the impact of mechanical segregation on the **thermal dispersion (temperatures heterogeneity)** in bi-size and bi-density beds of spherical milli-beads. The analysis was based on DEM simulations of flow and heat transfer in a rotating 'slice' type (nearly bi-dimensional) drum.

2. Theory and methods

The simulations of stirring and contact heating of milli-beads were realized with the commercial software EDEM 2017 (DEM Solutions, Edinburgh, UK). This software is based on the discrete elements method (DEM) which is a very powerful tool used more and more nowadays to investigate and develop granular solid processes. In the DEM framework, each particle of the granular bed is considered to be distinct and has its own trajectory and speed. The particle-particle and particle-boundary interactions are checked at each time step and the resulting individual particle positions are updated. The main assumption of DEM modeling is that the particles are rigid (non-deformable) solid bodies but having the capability of small interpenetration during their contacts. The resulting decrease of the distance between the centers of two adjoining particles is called the interpenetration depth (δ) or the overlap. This overlap is the fundamental variable which is directly related to the normal contact (interaction) force between the particles and the mechanical stiffness of the particles. It is also the basis for evaluating the heat conductance between the particles as described in the next sections.

2.1 Mechanical DEM modeling

The determination of the position and the speed of a given particle (identified by index i) is the time solution of the Newton second law for translational and rotational movement of a solid body. For translation, the dynamics of a single particle is then expressed as:

$$m_i \frac{d^2 \vec{x}_i}{dt^2} = \sum_j F_{ij} + m_i g \quad (1)$$

where m_i is the particle mass, x_i its position vector and the right hand side of the equation is the resulting force, cumulating interactions with all adjoining (j) particles (and the wall of the vessel) and gravity. A similar equation can be written for the rotational movement.

For the purpose of this study, default modeling option in EDEM, the Hertz-Mindlin contact model^[7] was used. In this model, the particle-particle mechanical interaction involves the normal impact force and the tangential friction force. This normal force is essentially elastic but both normal and tangential forces include damping components. The normal force is thus expressed by means of non linear visco-elastic behavior law:

$$F_{ij} = \alpha \delta_{ij}^{3/2} - \beta v_{ij} \quad (2)$$

where α is the elasticity or ‘stiffness’ coefficient depending theoretically on the material mechanical properties (essentially the Young’s modulus) and particles radius, β is the damping coefficient

depending on the **empiric restitution coefficient of the particles (ratio of relative velocity of two particles after collision to their relative velocity after collision)**, δ_{ij} is the overlap between particle i and j and v_{ij} is the relative velocity of the two particles. The maximal tangential friction force is given by the *Coulomb* law which involves a material dependent friction coefficient.

The overlap between two adjoining particles is a key variable because it determines the interaction mechanical force (equation 2) and the thermal conduction path (equation 3). While performing a DEM simulation this variable must be controlled. The particle ‘stiffness’ α is in fact an user defined simulation parameter. Its value is adjusted in order to limit the interpenetration depths to a desired fraction of the particle diameter, generally not more than 0.01, and at the same time to keep the minimal calculation time step as high as possible.

2.2 Thermal DEM modeling

In solid particulate systems several heat-transfer phenomena coexist between neighboring particles: direct solid-solid heat conduction, conduction and convection through the interstitial fluid and surface radiation. In this study, convection and radiation were neglected. The direct particle-particle conduction **was supposed to prevail over interstitial gas conduction** due to the high ratio of the solid particles intrinsic conductivity to the gas conductivity and due to moderate surface temperatures.

In DEM framework, as already stated in the preceding section, two particles in contact interpenetrate each other to a depth depending on their dynamics and their mechanical properties. For spherical

particles, the contact radius R_c , which is the radius of the circle resulting from the two particles (spheres) overlapping, can be straightly derived from the penetration depth. Approximate analytical solutions of the *Fourier* conduction equation between two smooth, elastic particles with a finite small contact area have been proposed in the literature^[5,6,7] and applied to evaluate the thermal conductance K_{ij} between the two particles centers. The resulting equation writes:

$$K_{ij} = 2\lambda_{ij}R_c = 2\lambda_{ij}\sqrt{R_{ij}}\sqrt{\delta_{ij}} \quad (3)$$

where λ_{ij} is the harmonic mean of the thermal conductivities of the two materials and R_{ij} is the harmonic mean of the particles radii. In this study, the most simple mechanical interaction model, i.e. the basic form of the Hertz model where the damping component of the normal force is not considered, was adopted for thermal simulation purposes, and the specific ‘hertz’ interpenetration depth was evaluated by:

$$\sqrt{\delta_{ij}^{He}} = \frac{1}{\sqrt{R_{ij}}} \left[\frac{3F_{ij}R_{ij}}{4E_{ij}} \right]^{1/3} \quad (4)$$

where E_{ij} represented an apparent particle-particle elasticity coefficient defined by:

$$\frac{1}{E_{ij}} = \frac{1-\nu_i^2}{E_i} + \frac{1-\nu_j^2}{E_j} \quad (5)$$

where E_i was the Young’s modulus of particle i and ν_i was the Poisson’s coefficient of particle i .

This thermal contact model is far from being very accurate and can be only considered as first approximation. Comparing the simulations results to experimental data and correcting the ‘thermal’ penetration depth will be needed to make the simulations predictive. Such a thermal DEM model calibration procedure was mentioned by Kwapinska et al. [2]. The effective thermal conductivity of the bed identified or experimentally measured in static bed conditions could be related to the particle to particle heat transfer coefficient used in DEM. Tsotsas [11] proposed very recently a new analytical equation for calculating particle-particle heat transfer coefficients from the effective thermal conductivity of respective packed beds. His formulation accounted for both direct solid and interstitial gas heat conduction between particles. In our study, only general qualitative trends of mechanical and thermal particles segregation were analyzed and the quantitative quality of the results was not sought or claimed **at the present stage**.

Once the delicate issue of evaluating the thermal conductances has been dealt with, the conductive heat flux between particle i and particle j writes simply:

$$\dot{Q}_{ij} = K_{ij}(T_j - T_i) \quad (6)$$

The total heat flux transferred to or from a given particle (i) is the sum of heat fluxes exchanged with all neighboring (j) particles and the thermal energy balance of a single particle writes :

$$m_i c_{pi} \frac{dT_i}{dt} = \sum_j \dot{Q}_{ij} \quad (7)$$

where c_{pi} is the particle specific heat capacity. The time integration of the above equation provides the thermal history of the considered particle.

In the case of a rotary drum considered here, the product was heated by the drum cylindrical lateral wall and the baffles inserted in that wall which were all maintained at a given operating temperature during the entire process (see figure 1). But the first product (particles) layer temperature is not equal to the wall temperature. Mathematically, if the particulate bed is considered as a continuous body, that corresponds to a boundary condition of the third kind (Robin's BC), with a prescribed transfer coefficient. Thus, the thermal model of the particulate bed has thus to include the thermal contact between the particles and the wall. In a general macroscopic approach, this thermal contact is described by a superficial heat transfer coefficient. In the DEM approach of this study, this issue was handled in the same way as the contact between two particles, by the Hertz direct solid-solid conduction model.

2.3 Particulate bed global characteristics

In order to characterize globally and macroscopically the geometrical distribution (mechanical segregation) of each kind of beads within the bed, statistical indexes already introduced in the literature^[3] were used. The mechanical segregation index was defined by :

$$MSI = \sqrt{\frac{1}{K-1} \sum_{i=1}^K (C_i - \langle C \rangle)^2} \quad (8)$$

where C_i was the fraction by number of one kind of beads (of the considered size or density) in a control volume i among K other control volumes, $\langle C \rangle$ was the average fraction by number of this kind of beads in the entire bed divided in K equal size control volumes ($K = 225$ in this study).

In order to quantify globally the thermal dispersion of the bed, the standard deviation of beads temperatures could be used as first choice:

$$\sigma_T = \sqrt{\frac{1}{N-1} \sum_{i=1}^N (T_i - \langle T \rangle)^2} \quad (9)$$

where T_i was the temperature of the bead i among all other beads, $\langle T \rangle$ was the overall temperature of the bed and N the total number of beads.

However, the thermal dispersion within segregated beds includes both the effect of the heating mode and the effect of mechanical segregation. In order to focus on the mechanical effect, a specific thermal segregation index was defined as the ratio between the standard deviation of the temperatures of the considered bi-dispersed (or gaussian dispersed) bed and the standard deviation of the temperatures of the mono-dispersed (not mechanically segregated) bed:

$$TSI = \frac{\sigma_T^{bi}}{\sigma_T^{mo}} \quad (9)$$

This index was plotted for different bed morphologies but for the same drum configuration (4 short baffles) on figure 2. This method could not be applied to the curves corresponding to all drum configurations studied because the simulation results for a monodispersed bed were not available for others baffles size and number. That's why on the other figures showing both the mechanical and thermal heterogeneity, the temperature standard deviation (σ_T) was simply used.

The overall bed temperature was not just a simple arithmetic average of the temperatures of all beads in the bed but was calculated as a heat capacity weighted average. For the bi-density bed the following formula was used :

$$\langle T \rangle = \frac{\sum_i^n M_{CA} C_{pCA} T_{CA}^i + \sum_j^m M_{PP} C_{pPP} T_{PP}^j}{\sum_i^n M_{CA} C_{pCA} + \sum_j^m M_{PP} C_{pPP}} \quad (10)$$

where n and m are respectively the numbers of cellulose acetate (CA) particles and of polypropylene (PP) particles, M is the mass of CA or PP particles, Cp is their specific heat capacity and T_{CA}^i and T_{PP}^j are their respective temperatures. Analogically, for the bi-size bed the overall temperature was given by:

$$\langle T \rangle = \frac{\sum_i^p M_{CA} C_{pCA} T_{CA}^i}{\sum_i^p M_{CA} C_{pCA}} \quad (11)$$

where p was the total number of CA particles.

2.4 Solver settings, material properties and process parameters

The simulations were realized on a DELL workstation (T7910) with two 10 cores processors (Intel Xeon E5-2660v3). The maximum processing time step was set at 40 % of the theoretical Rayleigh time step. This is the time taken for a shear wave to propagate through the particle which depends on the particle size and on its mechanical properties. The adjoining particles numerical search distance was set at 5 fold particle radius. The “Hertz-Mindlin with Heat Conduction model” was selected and an user-defined routine called “Heat conduction for Geometry” was incorporated for implementing particles-wall direct heat conduction.

The virtual (simulated) beds were composed of polypropylene (PP) spherical beads with 3 mm diameter (specifications according to Marteau & Lemarié, Sorbiers, France) and cellulose acetate (CA) spherical beads with 2 mm and 3 mm diameters (specifications according to CIMAP, Paris, France). The compositions of the four studied particulate beds are provided in Table 1. The gaussian dispersed bed was numerically generated with an average diameter of 3 mm and with 95 % of beads lying in a range from 2 to 4 mm.

Table 1

All materials mechanical and thermophysical properties needed for EDEM simulations are given in Table 2. The friction coefficients values for pairs of materials were obtained by model identification (fitting experimental data) and are given in Table 3. The drum used in this study was a ‘slice’ type one

with a large diameter to depth ratio (close to 7, with internal diameter of 300 mm and an internal depth of 42 mm).

Table 2

The front panel was made of glass, the rear one and the circular peripheral wall were made of stainless steel. Three baffles configurations were considered: a drum with no baffles, a drum equipped with 4 straight equidistant baffles with a height of 15 mm and a drum with 8 straight equidistant baffles of 40 mm. All these dimensions were reproduced from the experimental set-up used in our parallel experimental study (results not yet published). The default revolution speed was 3 rpm which corresponded to very slow rotation speeds often encountered for drying of fragile pharmaceuticals. The rotary drum *Froude* number was equal to 0.0015 corresponding to a ‘rolling’ flow mode. The drum filling volume ratio was set to 1/8 which corresponded to low product loads used in the industry for sensitive pharmaceutical materials. The initial beads temperature was 25 °C and the peripheral heating wall temperature constant set point was 50 °C.

Table 3

3. Results and discussion

The simulations were realized for the four types of bed and the three baffles configurations and are summarized in Table 4.

Table 4

The mechanical segregation index (MSI), the thermal segregation index (TSI), the temperature standard deviation (σ_T) and the overall bed temperature ($\langle T \rangle$), defined in section 2.3, were calculated with MATLAB from EDEM data extracted for each simulation and were plotted as function of time.

Figure 1

The mechanical and thermal distribution of beads at the front face of the bi-size bed (the face visible behind the glass window) are shown on figure 1. These images are for qualitative analysis purpose only. A clearly marked core of small and cold beads at the center of the bed and a peripheral layer of large and hot beads at the heating wall were observed. These observations were perfectly normal because mechanical segregation phenomenon made the smaller (or densier) beads converge by percolation (or by condensation) to the center of the bed [10] and because the bed was heated by the peripheral wall.

3.1 Comparing trends for different types of bed and same baffles configuration

Thermal segregation index (TSI) and overall bed temperature ($\langle T \rangle$) time evolutions for the four different beds studied (mono-dispersed, Gaussian-dispersed, bi-size et bi-density) are shown on figures 2 and 3. It is important to recall here that TSI was normalized in regard to the thermal dispersion due to boundary conditions and represents only the thermal dispersion resulting from mechanical mixing and segregation. What is striking on these plots is the fact that the beads spatial distribution impacted

strongly the thermal distribution only at the very beginning of the process. After two minutes, the TSI differences between beds of different morphologies remained but leveled off quite significantly.

According to these curves, the gaussian-dispersed bed presented the lowest TSI. This was probably due to the fact that poly-dispersed beads redistributed quite evenly, smaller beads occupying the spaces between larger ones, increasing bed apparent density (reducing bed porosity) and thus increasing the bed effective thermal conductivity. On the contrary, the bi-density bed showed the highest TSI. This behavior could be mainly explained by the fact that the bi-density bed exhibited the strongest mechanical segregation among all other beds morphologies in the quasi-steady stage. The other explanation could be that the bi-density bed was composed only of large beads of the same size (3 mm) and did not benefit from the thermal homogenization effect due to insertion of small beads among large beads. Besides, TSI curve for the bi-size bed with heated baffles and mono-dispersed beds were very close to each other. The curve for the bi-size bed with no heated baffles was very close to the one for gaussian bed. The case with not heated baffles exhibited a noticeably better thermal homogeneity than the one with heated baffles. This issue will be addressed in section 3.2.

Figure 2

In spite of the fact that both the bi-density bed and the mono-dispersed bed were composed of 3 mm beads, the TSI of the bi-density bed was much higher than that of the mono-dispersed one. This behavior could be attributed to the mechanical segregation: for a mono-dispersed bed there was no mechanical segregation at all and for the bi-density bed the mechanical segregation was very pronounced.

As concerns the overall bed temperatures ($\langle T \rangle$), plotted on Figure 3, the heating rate (represented by the temperature profile slope) was stronger for the bi-size bed than for the other beds. The overall temperature evolutions of bi-density and gaussian beds were very close to each other most likely because these two beds had the same mean bead diameter. That means that the beads size dispersion did not improve the heating rate, but mixing two populations as for the bi-size bed improved it. This could certainly be related to the effective thermal conductivity of the bed.

Despite the fact that there were much more small beads than large ones in the bi-size bed and that the smaller beads were preferentially in the colder core, the bi-size bed heated up faster than the bi-density one. As already mentioned, the possible explanation was that the smaller beads filled in the spaces between the larger ones in the bi-size bed. By consequence, the number of bead to bead and bead to wall contacts was increased and thus the bed effective thermal conductivity and beads-wall heat transfer coefficient were enhanced.

The above interpretation was very well supported by data concerning the total number of contacts between beads which were simulated by the software during one time step. This number was by far the highest for the bi-size bed with 90000 contacts per simulation time step, it reached 41 400 contacts for the mono-dispersed bed and 38 000 for the bi-density one. Even if the contacts numbers were rather close for the last two beds, a noticeable difference on the temperature curves could be observed. The contacts number appeared as a very good indicator for interpreting the heating kinetics of the bed. Of course, the number of contacts depends on the beads trajectories but also on the total number of beads. That is why the number of contacts difference between the bi-size bed (27905 beads) and the bi-density

(16238) and mono-dispersed (16238) was so important.

Figure 3

It is also worth noting that the TSI time evolutions for the bi-density bed corresponding to heated baffles and no heated ones were rather close and there was practically no difference at the end of the simulation. For the bi-size bed, the heated short baffles induced significantly more thermal segregation than the not heated ones. This will be discussed later. The heating rate was lower for cases with not heated baffles compared to the case with heated baffles.

3.2 Comparing trends for different baffles configurations but for same type of bed

The time evolutions of mechanical segregation index (MSI) and temperature standard deviation (σ_T) for the bi-size bed and the bi-density bed are respectively presented on figures 4 and 6. **It has to be pointed out that the standard deviation was not used here to assess the simulation error but to represent quantitatively the thermal dispersion within the bed.**

Generally, on both figures, two distinct stages (periods) were observed: before and after 3.5 minutes. MSI and σ_T curves presented similar shapes in the first stage where they passed through a maximum and different shapes in the second stage. In the second stage MSI tended to be stable after 8 minutes while σ_T decreased continuously and quite linearly. Thus, MSI and σ_T time profiles appeared possibly correlated during the first stage and not correlated in the second one. The first stage most likely corresponded to a transitory period when the beads were redistributed and the second one corresponded

to a quasi-steady period when the beads were already segregated. For longer times, σ_T tended logically to zero and MSI remained stable (results not shown).

σ_T decreased with increasing the number and the length of the baffles. Moreover the difference between case 4SB and case 8LB was larger than between 0B and 4SB, so that a kind of proportionality between σ_T level and the total surface area of the baffles was highlighted.

Figure 4

One of the major concerns of this study was to investigate the impact of mechanical segregation on thermal **dispersion**. This analysis was realized considering separately the two bi-dispersed beds and is described below.

3.2.1 Bi-size bed

According the bi-size bed simulation data, the initial and fast increase of MSI had a delayed but evident effect on σ_T which increased in its turn and reached a maximum 2 minutes after the MSI maximum. Regarding the effect of baffles configuration, σ_T globally decreased with increasing the number and the length of the baffles and the case 8LB appeared to be very efficient for the thermal homogenization of the bed.

However, if the global influence of mechanical segregation on thermal dispersion is considered, the trends were not straightforward to interpret. The case 4SB gave a very peculiar result since a higher MSI peak induced a lower σ_T peak when compared to the case 0B. For the case 8LB, MSI curve peak was the lowest compared to all other cases as well as the corresponding σ_T peak, what was rather comforting. However, because of the particular case 4SB, a direct correlation between MSI average level and σ_T average level was not observed. σ_T for case 0B case was higher than for case 4SBnh as expected, but σ_T for case 4SB (heated baffles) was unpredictably higher than for case 4SBnh (not heated baffles). The simulated images of the frontal face of the bed showed that some smaller beads were trapped in the angle between the wall and the baffle where they were rapidly overheated. This was possibly the reason why heated baffles could induce more local thermal gradients than not heated ones.

Figure 5

As concerns the influence of the baffles on the overall bi-size bed temperature variation (see figure 5), the heating rate increased with the number and the length of the baffles. Logically, the heating rates (represented by the slope of the curve) were proportional to the heating (beads-wall) surface area and thus to the surface area of the baffles. Nevertheless, while the case 8LB exhibited a significant heating speed-up, the case 4SB had a rather moderate impact compared to the case 0B and the case 4SBnh had practically no impact at all. Short not heated baffles appeared to be useless for accelerating the heating process. This was not really surprising because the total heating surface area was in fact the same for configuration 0B and configuration 4SBnh.

3.2.2 Bi-density bed

Unlike for the bi-size bed, there was no marked peak on MSI curves. MSI increased and reached a plateau rapidly but monotonically. The maxima of σ_T curves were also less pronounced. As like for the bi-size bed, σ_T was significantly reduced by increasing the number and the length of the baffles, independently of the fact that MSI increased between case 0B and case 4SB. Moreover for the bi-density bed the MSI for case 8LB was higher than for the case 0B. Thus, the baffles improved the thermal homogeneity of the bed but did not improve its mechanical homogeneity. Therefore, no correlation between the average MSI level and the average σ_T level was found. σ_T for cases 4SB (heated baffles) and case 4SBnh (not heated baffles) converged very closely at the end of the simulation.

Figure 6

As concerns the influence of the baffles on the overall bi-density bed temperature variation (see figure 7), the heating rates increased with the number and the length of baffles as for the bi-size bed. The case 8LB provided the highest rate and all other baffles configurations exhibited much lower rates. It must be noted that case 4SBnh was even less efficient than 0B, what corroborated the conclusion already pointed out for the bi-size bed that not heated baffles did not improve the heating rate of the particulate bed.

Figure 7

4. Conclusion

Mechanical flow and heat transfer phenomena within a bed composed of milli-metric size spherical beads rotated and heated by contact in a horizontal drum were investigated. The mechanical segregation index (standard deviation of local bed compositions), the standard deviation of beads temperatures and the thermal segregation index (normalized standard deviation) were calculated by means of the DEM method for four very different types of beds: mono-dispersed, gaussian-dispersed, bi-size and bi-density. Different baffles configurations: no baffles, 4 short baffles and 8 long baffles, were also studied.

The temperatures dispersion was found to be enhanced by the mechanical segregation and was stronger for bi-dispersed beds than for mono-dispersed and gaussian ones, especially for the bi-density bed. But, the thermal heterogeneity level did not follow straightforwardly the morphological heterogeneity level. For instance, the significant increase of the mechanical segregation index when passing from a drum without baffles to a drum with short baffles was not observed on the thermal dispersion curves. Globally, no direct correlation between the average mechanical segregation level and the average thermal dispersion level was demonstrated.

The overall heating rate was much faster for the bi-size bed than for the other beds. The overall temperature time profiles of bi-density and gaussian beds were very close to each other. The baffles configuration had an important influence on the thermal evolution of the bed. When the number and length of baffles were increased, the thermal dispersion level was decreased nearly proportionally to

the baffles total surface area. But the heating rate was not really proportional to baffles surface area and was significantly improved only for the longest baffles. Not heated short baffles had no effect.

In order to carry on with this study, the thermal DEM simulations will have to be validated by means of experiments or results from literature. Especially, the evaluation of particle to particle heat conductances will have to be reconsidered so that the DEM model becomes more quantitatively accurate and really predictive. Then, the next step of our work will be modeling and DEM implementation of the water vaporization and desorption within wet beads with the aim of simulating a contact rotary drying process. This would be of highest importance for developing efficient but more product careful technologies for drying of crops, particulate food or pharmaceutical powders.

References

- [1] Schlünder, E.-U.; Mollekopf N. Vacuum contact drying of free flowing mechanically agitated particulate material. *Chemical engineering and processing: Process Intensification* 1984, 18(2), 93-111.
- [2] Kwapinska, M.; Saage, G.; Tsotsas, E. Continuous versus discrete modelling of heat transfer to agitated beds. *Powder Technology* 2008, 181(3), 331–342.
- [3] Figueroa, I.; Vargas, W.L.; McCarthy, J.J. Mixing and heat conduction in rotating tumblers. *Chemical Engineering Science* 2010, 65(2), 1045–1054.
- [4] Chaudhuri, B.; Muzzio, F.J.; Tomassone, M.S. Experimentally validated computations of heat transfer in granular materials in rotary calciners. *Powder Technology* 2010, 198(1), 6–15.

- [5] Gui, N.; Gao, J.; Ji, Z. Numerical study of mixing and thermal conduction of granular particles in rotating tumblers. *AIChE Journal* 2012, 59(6), 1906–1918.
- [6] Komossa, H.; Wirtz, S.; Scherer, V.; Herz, F.; Specht, E. Heat transfer in indirect heated rotary drums filled with monodisperse spheres: Comparison of experiments with DEM simulations. *Powder Technology* 2015, 286, 722–731.
- [7] Emady, H.N.; Anderson, K.V.; Borghard, W.G.; Muzzio, F.J.; Glasser, B.J.; Cuitino, A. Prediction of conductive heating time scales of particles in a rotary drum. *Chemical Engineering Science* 2016, 152, 45–54.
- [8] Nafsun, A.I.; Herz, F.; Specht, E.; Komossa, H.; Wirtz, S.; Scherer, V.; Liu, X. Thermal bed mixing in rotary drums for different operational parameters. *Chemical Engineering Science* 2017, 160, 346-353, <https://doi.org/10.1016/j.ces.2016.11.005>
- [9] Nafsun, A.I.; Herz, F.; Liu, X. Influence of material thermal properties and dispersity on thermal bed mixing in rotary drums, *Powder Technology* 2018, 331, 121-128, <https://doi.org/10.1016/j.powtec.2018.01.072>
- [10] Félix, G.; Falk, V.; D'Ortona U. Segregation of dry granular material in rotating drum: experimental study of the flowing zone thickness. *Powder Technology* 2002, 128(2-3), 314-319, [https://doi.org/10.1016/S0032-5910\(02\)00171-7](https://doi.org/10.1016/S0032-5910(02)00171-7)
- [11] Tsotsas, E. Particle-particle heat transfer in thermal DEM: Three competing models and a new equation. *International Journal of Heat and Mass Transfer* 2019, 132, 939-943, <https://doi.org/10.1016/j.ijheatmasstransfer.2018.12.090>

Figures R1

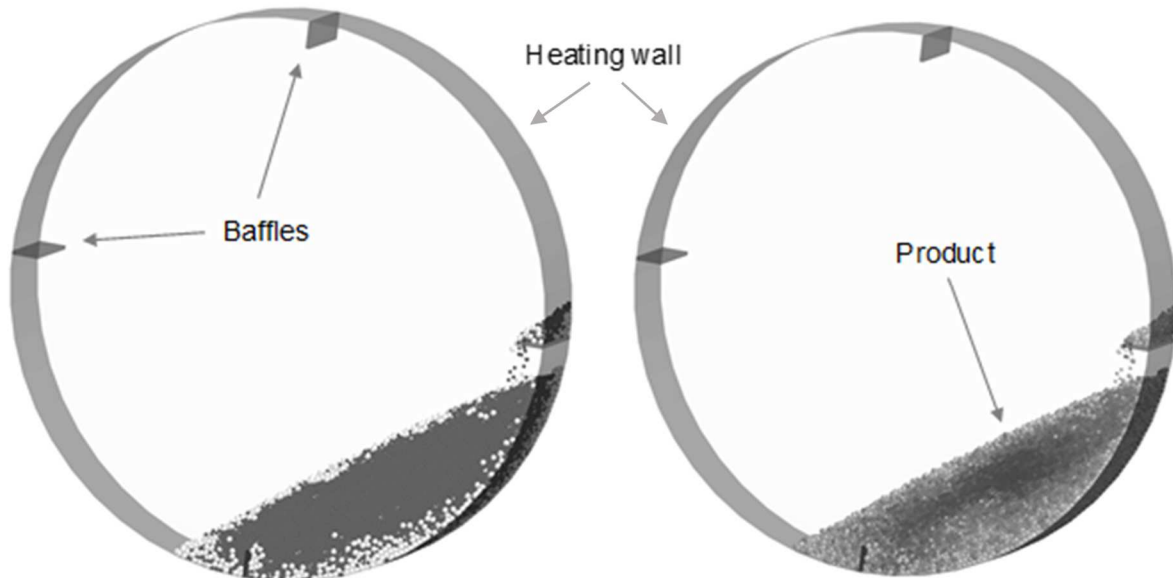


Figure 1. **Simplified scheme of the drum with milli-beads distributions visualization** for the bi-size bed after 8 minutes of drum rotation (24 revolutions) : on the left the small beads are black and the large ones are white, on the right the cold beads are darker and the hot ones are clearer.

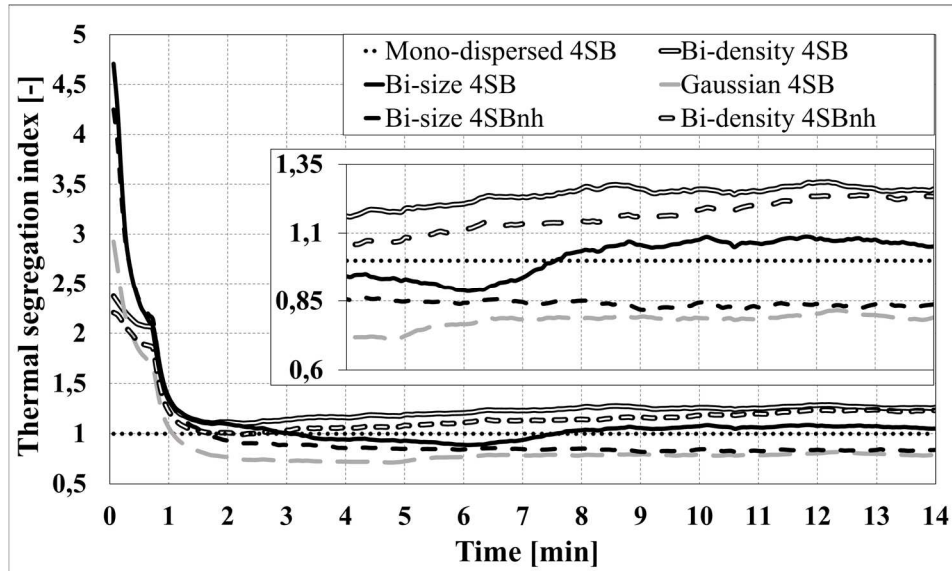


Figure 2. Thermal segregation index versus time for all bed types and for short baffles.

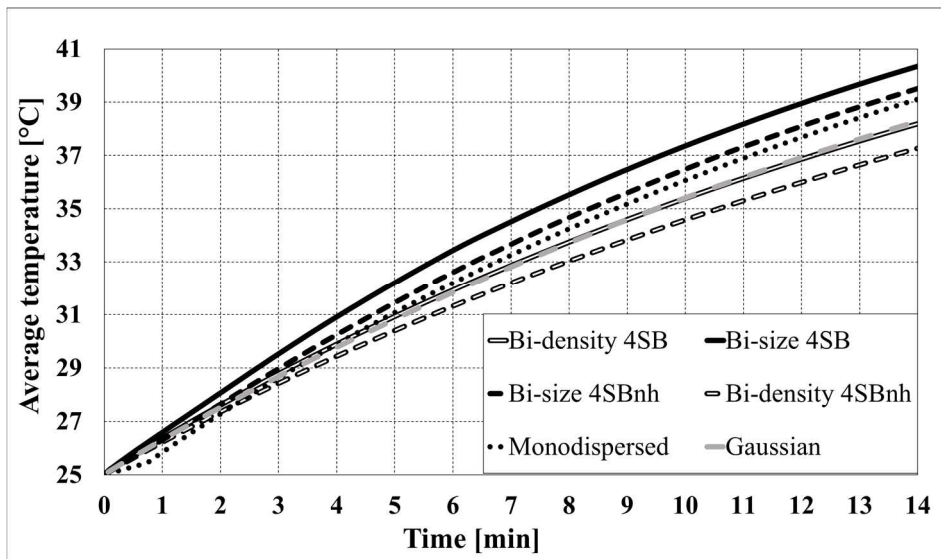


Figure 3. Overall bed temperature ($\langle T \rangle$) versus time for all bed types and for short baffles.

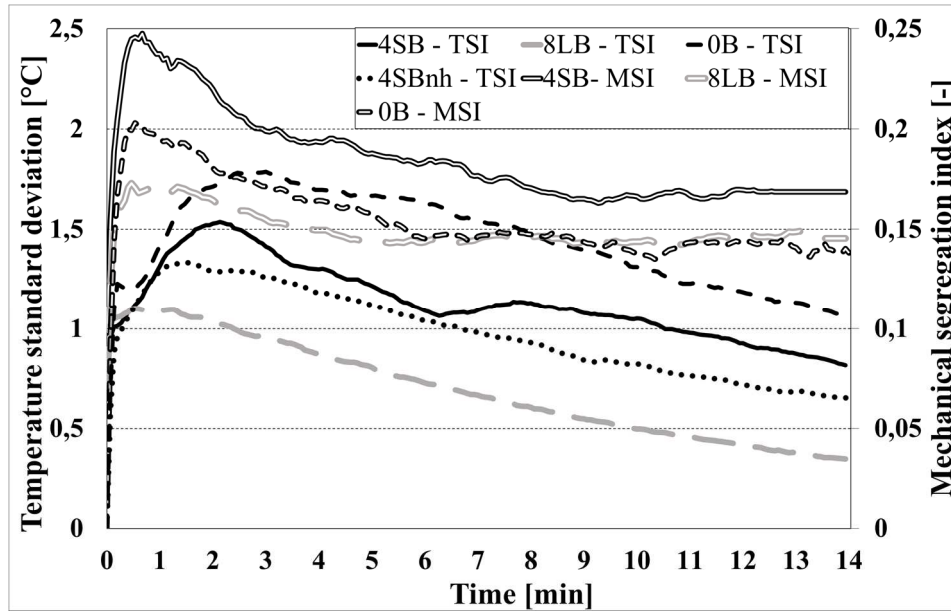


Figure 4. Mechanical segregation index (MSI) and **thermal dispersion (σ_T) coefficient** versus time for the bi-size bed and for all baffles configurations.

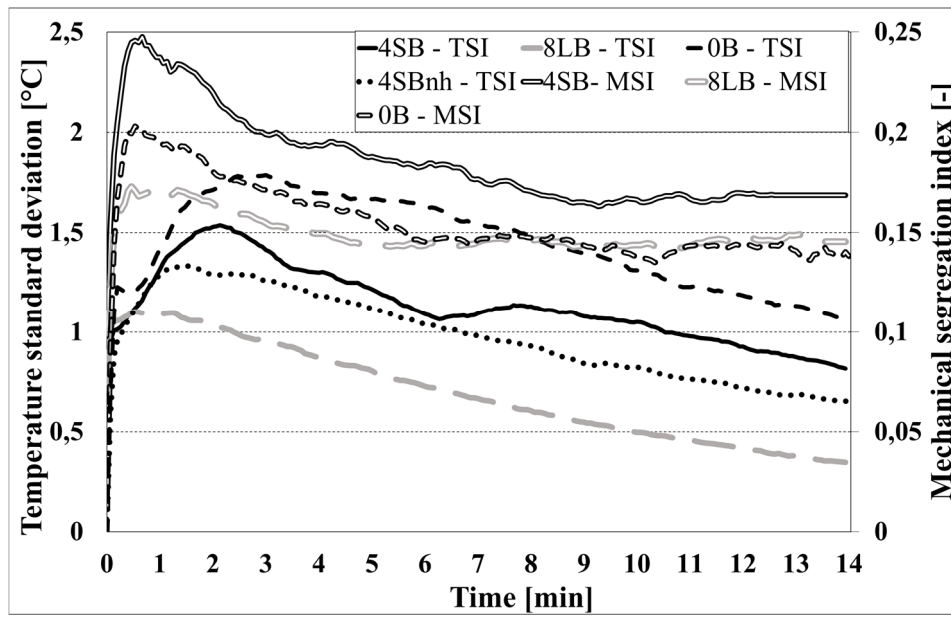


Figure 5. Overall temperature ($\langle T \rangle$) versus time for the bi-size bed and for all baffles configurations.

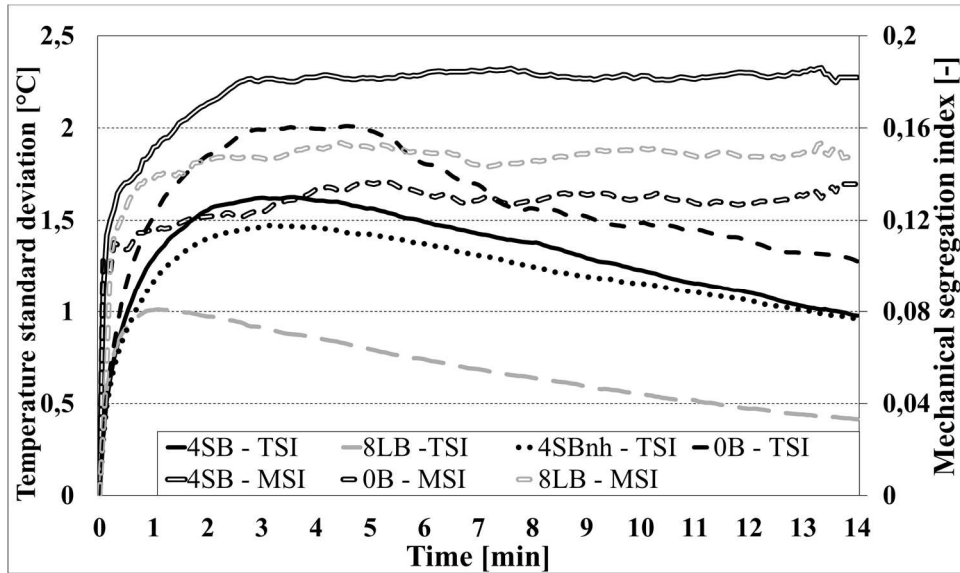


Figure 6. Mechanical segregation index (MSI) and **thermal dispersion (σ_T) coefficient** versus time for the bi-density bed and for all baffles configurations.

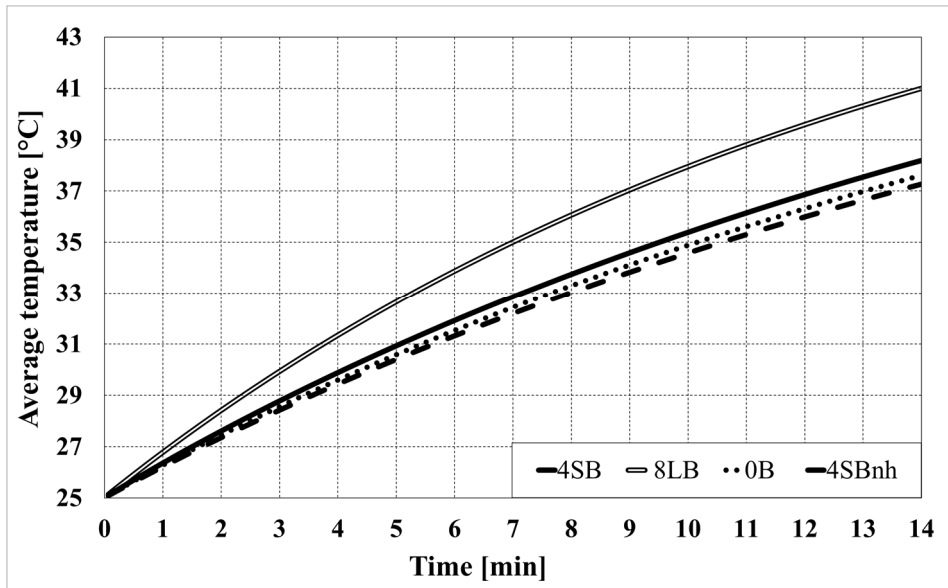


Figure 7. Overall temperature ($\langle T \rangle$) versus time for the bi-density bed and for all baffles configurations.

Tables

Table 1. Beads number for different bed types.

	Mono-dispersed	Bi-density	Bi-size	Gaussian
CA Ø 2			27905	
CA Ø 3	16366	8183	8183	
PP Ø 3		8055		
CA Ø 3±1				16366

Table 2. Materials thermal and mechanical properties

BEADS	Property	Units	CA	PP
	Density ^a	[kg/m ³]	1280	910
	Poisson's ratio ^a	[-]	0.4	0.42
	Elastic modulus [*]	[MPa]	2.8	2.84
	Shear modulus [*]	[MPa]	1	1
	Thermal conductivity [*]	[W/(m.K)]	1	1
	Specific heat capacity ^b	[J/(kg.K)]	1200	1700
	Coefficient of rolling friction ^c	[-]	0.01	0.01
	Coefficient of restitution ^c	[-]	0.3	0.3
DRUM			Steel	Glass
	Density ^b	[kg/m ³]	7800	2500
	Poisson's ratio ^b	[-]	0.3	0.21
	Elastic modulus ^b	[GPa]	182	94.3
	Shear modulus ^b	[GPa]	70	39
	Thermal conductivity ^b	[W/(m.K)]	15	0.93
	Specific heat capacity ^b	[J/(kg.K)]	502	/
	Coefficient of rolling friction ^c	[-]	0	0.01
	Coefficient of restitution ^c	[-]	0.3	0.3

a - manufacturers data, b - free access web data, c - data from this study,

* user defined value for speeding up the simulations

Table 3. Solid-solid static friction coefficients

	Bead- Steel	Bead- Glass	Bead-Bead	
			CA	PP
CA	0.3	0.2	0.3	0.6
PP	0.3	0.2	0.6	0.6

Table 4. Layout and referencing of thermal DEM simulations

Bed	Bi-size			Bi-density			Gaussian	Mono-dispersed
Baffles geometry (number * height in cm)	0	4*1.5	8*4	0	4*1.5	8*4	4*1.5	4*1.5
Heating of baffles	Yes	Yes No	Yes	Yes	Yes No	Yes	Yes	Yes
Case reference (on figures and in the text)	0B	4SB 4SBnh	8LB	0B	4SB 4SBnh	8LB	4SB	4SB

